Human Molecular Genetics, 2009, Vol. 18, No. 16 **2975–2988**
doi:10.1093/hmg/ddp236
Advance Access published on May 19, 2009

Diet-induced hepatocellular carcinoma in genetically predisposed mice

Annie E. Hill-Baskin[1,†], Maciej M. Markiewski[2,†], David A. Buchner[1,†], Haifeng Shao[1,†], David DeSantis[3], Gene Hsiao[4], Shankar Subramaniam[4], Nathan A. Berger[5,6], Colleen Croniger[3,†], John D. Lambris[2,‡] and Joseph H. Nadeau[1,5,6,*,‡]

[1]Department of Genetics, Case Western Reserve University School of Medicine, Cleveland, OH 44106, USA, [2]Department of Pathology and Laboratory Medicine, University of Pennsylvania, Philadelphia 19104, USA, [3]Department of Nutrition, Case Western Reserve University School of Medicine, Cleveland, OH 44106, USA, [4]Department of Bioengineering, University of California, San Diego, CA 93093, USA, [5]Case Center for Transdisciplinary Research on Energetics and Cancer and [6]Case Comprehensive Cancer Center, Case Western Reserve University School of Medicine, Cleveland, OH 44106, USA

Received January 5, 2009; Revised and Accepted May 14, 2009

Hepatocellular carcinoma (HCC) is one of the leading causes of cancer death worldwide, with ~70% of cases resulting from hepatitis B and C viral infections, aflatoxin exposure, chronic alcohol use or genetic liver diseases. The remaining ~30% of cases are associated with obesity, type 2 diabetes and related metabolic diseases, although a direct link between these pathologies and HCCs has not been established. We tested the long-term effects of high-fat and low-fat diets on males of two inbred strains of mice and discovered that C57BL/6J but not A/J males were susceptible to non-alcoholic steatohepatitis (NASH) and HCC on a high-fat but not low-fat diet. This strain–diet interaction represents an important model for genetically controlled, diet-induced HCC. Susceptible mice showed morphological characteristics of NASH (steatosis, hepatitis, fibrosis and cirrhosis), dysplasia and HCC. mRNA profiles of HCCs versus tumor-free liver showed involvement of two signaling networks, one centered on Myc and the other on NFκB, similar to signaling described for the two major classes of HCC in humans. miRNA profiles revealed dramatically increased expression of a cluster of miRNAs on the X chromosome without amplification of the chromosomal segment. A switch from high-fat to low-fat diet reversed these outcomes, with switched C57BL/6J males being lean rather than obese and without evidence for NASH or HCCs at the end of the study. A similar diet modification may have important implications for prevention of HCCs in humans.

INTRODUCTION

Hepatocellular carcinoma (HCC) is the fifth most common cancer and the fourth leading cause of cancer death worldwide (1). Most cases result from hepatitis B and C viral infection, aflatoxin exposure, chronic alcohol use and genetic liver diseases, such as primary hemachromatosis and Wilson disease (2). However, an increasing number of cases is associated with obesity, type 2 diabetes and related metabolic diseases, such as non-alcoholic steatohepatitis (NASH) (3,4). In general, the molecular and cellular mechanisms that are responsible for liver damage, neoplastic transformation of hepatocytes and HCC development are poorly understood for these various etiologies. HCCs associated with NASH are thought to develop through a continuous transition of liver pathologies, which begins with steatosis and proceeds through hepatitis, fibrosis and cirrhosis, and ends with benign liver tumors and HCC (3–5). It has been proposed that liver damage resulting from NASH leads to cycles of liver cell dedifferentiation, regeneration, proliferation and ulti-

*To whom correspondence should be addressed at: Department of Genetics, BRB731, CWRU, 10900 Euclid Ave, Cleveland, OH 44106, USA. Email: joseph.nadeau@case.edu or jhn4@case.edu
†These authors contributed equally to the work reported in this paper.
‡These authors co-supervised this work.

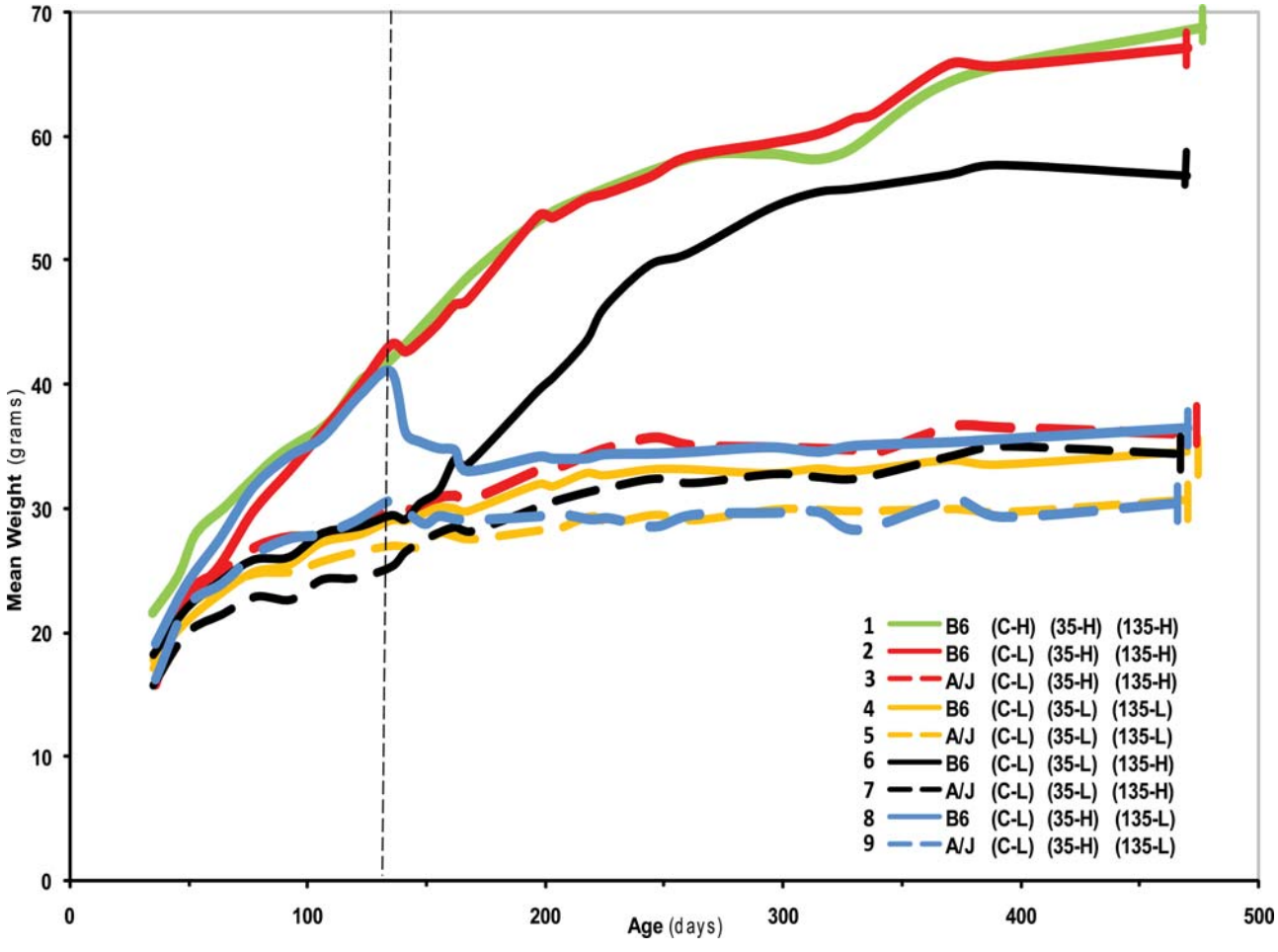

Figure 1. Patterns of weight gain. Males were weighed at 2 week intervals. Vertical dashed lines at 135 days show the points when diets were switched from H to L or from L to H chow for groups of A/J and C57BL/6J males. Vertical bars show the SEM at the end of the study. See the legend of Table 1 for details.

mately neoplastic transformation (3–5). Characterizing pathogenesis and testing for convergence among down-stream pathways of the various initiating conditions are important for understanding mechanisms leading to HCCs, identifying diagnostic markers and developing prophylactic measures and effective treatments.

We investigated the long-term effects of a high-fat diet in an established model of diet-induced metabolic disease (6) and discovered that C57BL/6J but not A/J inbred mice are susceptible to NASH and HCC. We also found that a switch from high-fat to low-fat diet after onset of fatty liver disease reversed outcome with no evidence for HCC at the end of the study.

RESULTS

Susceptibility of C57BL/6J males to diet-induced obesity

Previous studies showed that C57BL/6J males, and to a lesser extent females, are predisposed to diet-induced obesity and non-alcoholic fatty liver disease (NAFLD). However, these studies focused only on short-term responses to high-fat diets (6,7). To test the long-term effects of fatty diets, we introduced C57BL/6J and A/J males to high-fat (H) versus low-fat (L) diet according to various protocols and then followed these groups until we found evidence for weight loss or deteriorating health, at which point all mice were sacrificed. For this study, males from both strains were divided into groups (numbered 1–9) according to the time when the H or L diet was introduced (Fig. 1). By the end of the study, C57BL/6J males fed the H diet from conception (group 1), 35 days (group 2) or 135 days of age (group 6) developed clinically overt obesity as demonstrated by significant increases in body weight (Fig. 1) and body mass index (BMI) (Table 1). Interestingly, the switch from the H to L diet at 135 days of age in C57BL/6J males, which had been on H diet from 35 days of age (group 8), prevented the development of obesity by the end of study, even though these mice were heavier than C57BL/6J males on L diet (group 4) at day 135 (Fig. 1; Table 1). C57BL/6J on the L diet (group 4) as well as A/J males on various diet regimens (groups 3,5,7,9) remained lean throughout the study (Fig. 1; Table 1). These results clearly demonstrate that susceptibility to diet-induced obesity depends on both genetic background and diet. In addition, the time at which the H diet was introduced to C57BL/6J males had little impact on final body weight. However, the switch from H to L diet at day 135 protected C57BL/6J males from obesity despite a significant initial weight gain.

Table 1. Body weight in A/J and C57BL/6J males

Group	Strain	Diet: C-35 days, 35–135 days, 135 day-end	*N* (35 days)	*N* (∼400 days)	IW (g)	PA (day)	PW (g)	FW (g)	Final BMI (g/cm^2)	Comment
2	C57BL/6J	LHH	10	9	17.58 ± 0.44	417	67.98	64.16 ± 3.69	0.58 ± 0.02	Obese
6	C57BL/6J	LLH	10	5	18.24 ± 0.47	324	52.83	49.21 ± 4.23	0.54 ± 0.04	Obese
1	C57BL/6J	HHH	23	16	21.55 ± 0.52	420	65.80	64.38 ± 2.52	0.53 ± 0.02	Obese
3	A/J	LHH	10	9	15.83 ± 0.28	325	37.60	34.36 ± 1.85	0.34 ± 0.02	Lean
8	C57BL/6J	LHL	10	10	19.05 ± 0.26	167	41.87	36.50 ± 1.19	0.33 ± 0.01	Lean
7	A/J	LLH	10	10	15.74 ± 0.72	428	35.49	34.30 ± 2.08	0.33 ± 0.02	Lean
4	C57BL/6J	LLL	10	10	17.77 ± 0.40	366	34.68	34.15 ± 0.78	0.31 ± 0.01	Lean
9	A/J	LHL	10	9	16.17 ± 0.43	265	32.27	29.60 ± 1.08	0.28 ± 0.01	Lean
5	A/J	LLL	10	8	17.16 ± 0.21	380	30.59	29.72 ± 1.35	0.28 ± 0.01	Lean

Group numbers were used to highlight patterns with weight gain (Fig. 1). Diet sequence: C, 35 day and 135 day—diet introduced at conception, 35 days of age and 135 days of age, respectively. *N*, sample size at the designated time-point. H, high-fat chow; L, low fat chow; IW, initial weight (g) at 35 days; PA, age (days) at peak weight; PW, weight (g) at peak age; FW, body weight (g) at sacrifice, final BMI, body mass index (g/cm^2) at the end of the study; Mean ± SEM, standard error of the mean. Results are ranked according to final BMI from high to low.

NASH, liver dysplasia and HCC in obese C57BL/6J males

As expected, males with high BMI showed significant subcutaneous, peritoneal and thoracic adiposity at the end of the study (data not shown). Livers from these mice were pale and enlarged (hepatomegaly) in comparison to those in lean males. In addition, we frequently observed tumors of various diameters on the liver surface (Fig. 2). Gross examination revealed nodular lesions, suggesting malignant growth, in ∼70% of the C57BL/6J males that had been maintained on the H diet (Figs 2 and 3). In contrast, lean males, regardless of strain, did not show obvious liver pathology or nodular lesions.

Because gross examination of livers from obese mice suggested NASH, several histological features of liver disease were evaluated (Fig. 4). In a majority of obese C57BL/6J males, microscopic examination of liver sections demonstrated typical features of NASH in various stages of development including simple steatosis, inflammation, fibrosis and cirrhosis. Moderate to severe micro- and macro-vesicular steatosis was frequently observed (Fig. 4A). In some livers, steatosis was associated with mixed intra-lobular inflammatory infiltrate (Fig. 4A), various degrees of fibrosis (Figs 4B–D) and hepatocyte injury represented by Mallory hyaline (Fig. 4E) and ballooning degeneration (Fig. 4F). These features were consistent with the diagnosis of NASH. Occasionally, liver fibrosis was extensive with the formation of collagen bands connecting neighboring portal triads, central veins or portal triads with central veins, suggesting evolution of NAFLD toward cirrhosis (Fig. 4D). However, fully developed cirrhosis was rarely seen. Other features associated with but not diagnostic for NASH such as intranuclear inclusions (Fig. 3G) and ductular reaction (Fig. 4H) were also seen. Liver sections from C57BL/6J mice on L chow and A/J mice regardless of diet (Fig. 4I and J) showed in most cases normal liver histology.

Histological examination of livers from obese C57BL/6J males frequently revealed microscopic foci of liver cell dysplasia without grossly visible nodules (Fig. 5A). Focal nodular lesions found during gross examination showed features of low- or high-grade dysplasia (Fig. 5B–E) or well-differentiated HCC (Fig. 5F–H). Importantly, dysplastic nodules as well as HCCs were observed in livers without pre-existing cirrhosis. The occurrence of dyplastic and cancerous lesions in livers, which showed morphological features of NASH without fully developed cirrhosis, indicates that the same factors, which are responsible for the development of NASH, contribute to transformation of malignant liver cells (Fig. 3). HCCs without cirrhosis are not unusual in humans or mice (8–10). Together, these findings strongly suggest that liver cirrhosis was not a prerequisite for the development of HCC, especially in the presence of NASH.

Biomarkers of NAFLD and NASH

A panel of biomarkers was typed to characterize the metabolic features of liver disease in C57BL/6J males (Table 2). Fasting glucose was significantly elevated but not to hyperglycemic levels in C57BL/6J males that were fed the H diet. In contrast, A/J mice had similarly low blood glucose levels on the H and L diets. In contrast, the significant elevation of fasting plasma insulin levels suggests that C57BL/6J males may be insulin-resistant on the H diet. Further studies are needed to test for insulin sensitivity. Elevated plasma and hepatic triglycerides are often associated with obesity and insulin resistance (11). Interestingly, plasma triglycerides were normal but hepatic triglycerides were elevated on the H diet when compared with published results for C57BL/6J males fed L diet (12). Elevated hepatic triglycerides may result from increased fatty acid synthesis or oxidation (8–10). We therefore measured the mRNA levels of selected fatty acid synthesis genes as well as fatty acid oxidation genes (Table 2). C57BL/6J males fed the H versus L diets showed significantly reduced transcript levels for fatty acid synthesis and fatty acid oxidation genes, whereas A/J males had reduced transcript levels for fatty acid synthesis genes on the H versus L diet.

Inflammation and oxidative stress in the liver are associated with NASH and obesity (8–10). The potential sources of reactive oxygen species include hepatic cytochrome P4502E1 (CYP2E1) (10). We found that C57BL/6J and A/J males that were fed the H and the L diet showed no change in C4P2E1 levels (Table 2). However, hepatic TNFα concentrations were elevated in C57BL/6J males that were fed the H diet.

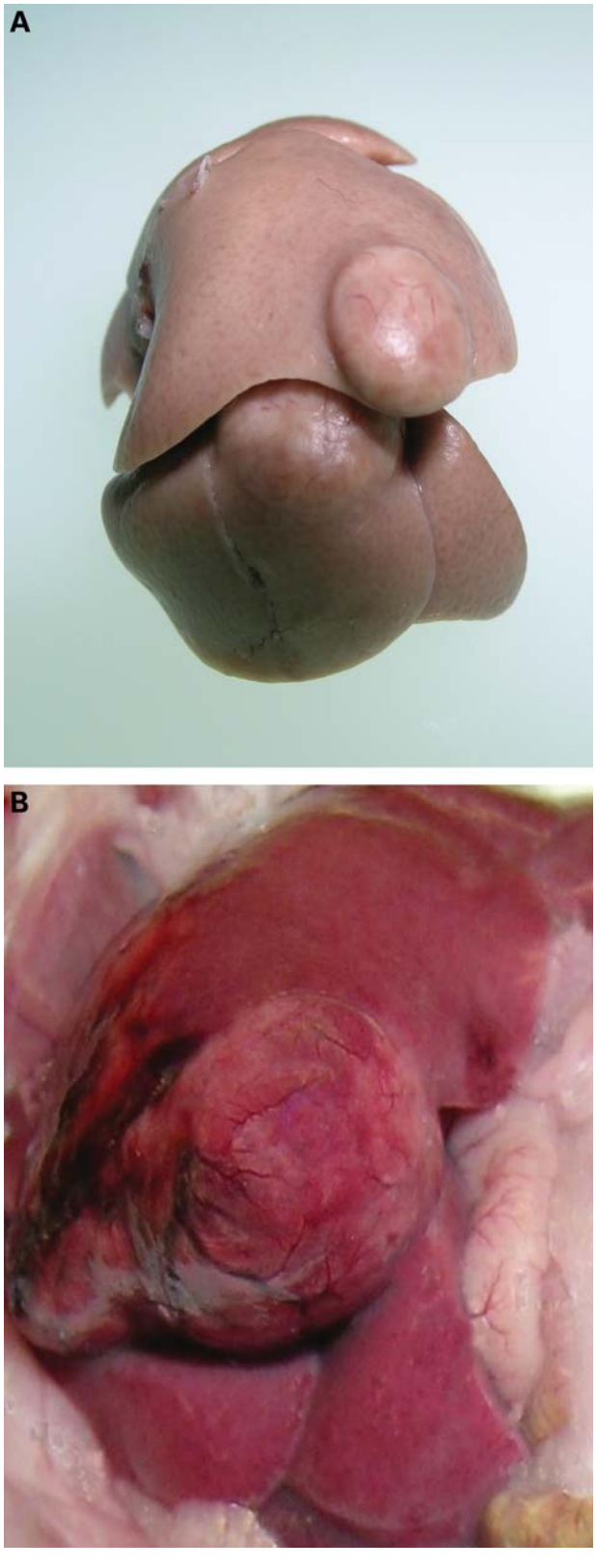

Figure 2. Examples of a nodule (**A**) and an HCC (**B**).

Oxidative stress and increased TNFα can damage mitochondria and result in liver injury. We therefore measured plasma levels of alanine aminotransferase (ALT) (13) as an indicator of liver injury and found increased ALT concentrations in C57BL/6J males fed the H diet, but not in A/J males regardless of diet. Together, these results show that the H diet resulted in steatosis, and liver injury in C57BL/6J males on the H but not the L diet, whereas A/J males were protected from the liver injury on the H diet.

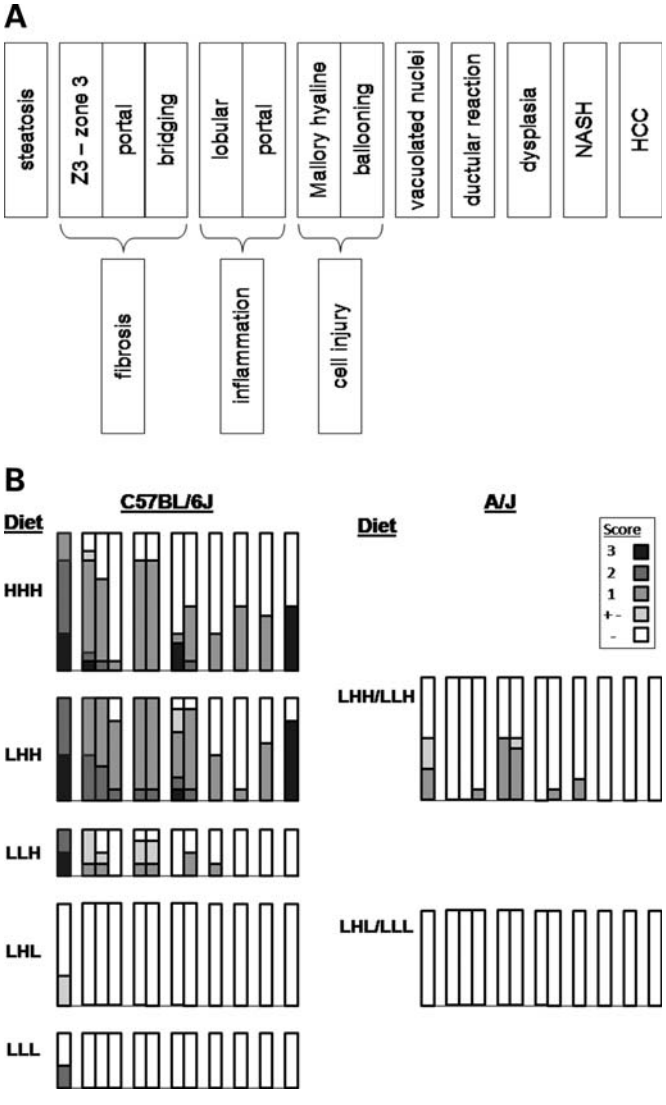

Figure 3. Frequency of histological features and pathological conditions. (**A**) Reference features. (**B**) Frequency of features. Sequence of diets—conception, 35 days of age and 135 days of age; H, high fat and L, low fat. Features in each sample were scored on the scale that is shown. The percentage of males in each group is provided with a *Y*-axis scale that ranges from 0 (bottom) to 100% (top). Information about diet composition can be found in the Materials and Methods.

mRNA expression profiles in diet-induced mouse HCCs

Genome-wide mRNA expression analysis, using the VAMPIRE algorithm (14,15), revealed 216 unique genes, many of which are involved in lipid metabolism, that were differentially expressed between paired samples of tumor-free liver and diet-induced HCCs from the same mice (Supplementary Material, Table S2). Gene set enrichment analysis (GSEA;

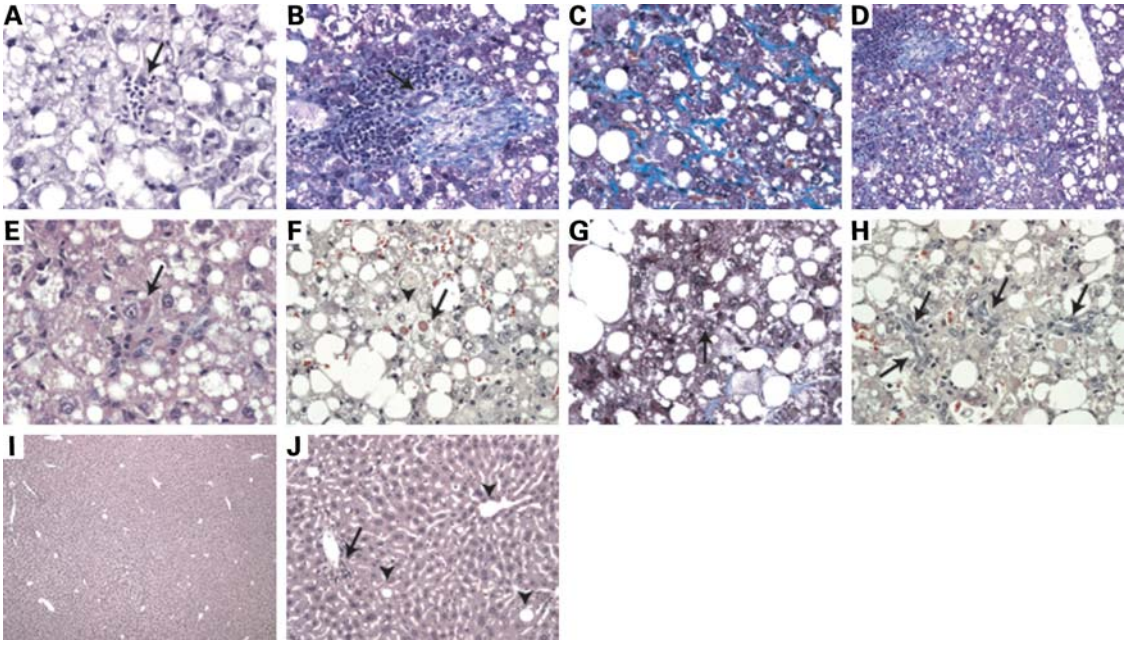

Figure 4. Development of NASH. (**A**–**H**) Histopathological features of NASH in livers of C57BL/6J mice fed high-fat (H) chow. (**I-J**) Normal morphology of livers from A/J mice fed H chow. (A) Mixed intralobular inflammatory infiltrate (arrow) in fatty liver (H&E, ×400). (B) Pronounced inflammatory infiltrate composed of mononuclear cells and blue wave-like bands of fibrotic tissue visualized by Masson's trichrome stain in the portal region; an arrow points to a bile duct (Masson's trichrome, ×400). (C) Perivenular and pericellular fibrosis (blue) in zone 3 (Masson's trichrome, ×400). (D) Bands of fibrotic tissue (blue) connect several portal triads (bridging fibrosis) (Masson's trichrome, ×200). (E) Mallory hyaline visible in the cytoplasm of degenerating hepatocyte (arrow) (H&E, ×600). (F) Ballooning degeneration of hepatocytes (arrow head) and giant mitochondria visible as round red cytoplasmic inclusions (arrow) (H&E, ×400). (G) Intra-nuclear inclusion (arrow) (Masson trichrome, ×400). (H) Ductular reaction in portal triad, arrows point to hypertrophic, proliferating bile ducts (H&E, ×400). (I) Normal morphology of liver (H&E, ×40) from an A/J mouse. (J) Unaltered portal triad (arrow) and central veins (arrow heads) from the same mouse (H&E, ×200).

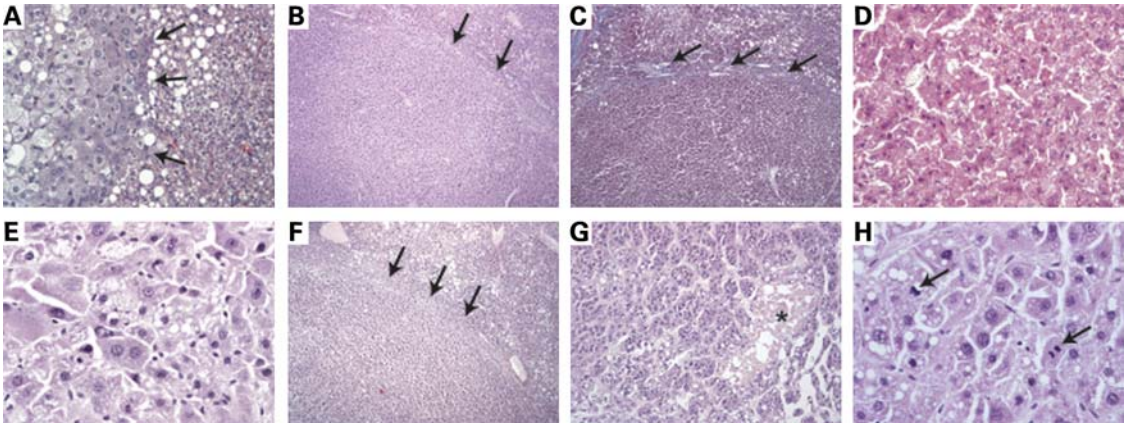

Figure 5. Pre-neoplastic and neoplastic lesions in livers from C57BL/6J males fed high-fat (H) chow. (**A**) Low-grade dysplastic changes found in the liver with features of NASH; arrows point to the border between dysplastic and non-dysplastic liver parenchyma (H&E, ×400). (**B**) A nodular lesion compressing surrounding the parenchyma (bulging growth) in a liver with histological features of NASH; arrows point to the border between a nodule and the remaining parenchyma (H&E, ×40). (**C**) The same nodule as shown in (B); arrows point to the fibrotic tissue separating the lesion from surrounding liver tissue (Masson's trichrome, ×40). (**D**) Plate thickening and small cell dysplasia in a nodular lesion found in a liver with NASH (H&E, ×200). (**E**) Significant cellular atypia observed in the nodular lesion found in a liver with NASH (H&E, ×400). (**F**) Hepatocellular carcinoma (HCC), which developed in a liver with NASH, compressing surrounding liver parenchyma (H&E, ×40). (**G**) Pseudo-glandular structures and necrosis (asterisk) in HCC shown in F (H&E, ×200). (**H**) Mitotic activity in the same HCC as shown in (F) and (G); arrows point to mitotic figures (H&E, ×400).

ref. 16) revealed a single curated set of 69 genes that was enriched in the tumor samples, many of which are commonly up-regulated in undifferentiated cancers relative to well-differentiated cancers (fdr < 0.025; Fig. 6; see also ref. 17 for a description of the way that the set of 69 genes was obtained from a meta-analysis of the Oncomine gene expression database). Differential expression of lipid metabolism genes and predominance of markers for poorly differentiated hepatocytes is consistent with both loss of lipid metabolic function and the histological and biomarker analysis.

Table 2. Biomarkers for fasting C57BL/6J and A/J males on L or H diet

Trait	B6 low fat, Mean ± SEM (*n*)	B6 high fat, Mean ± SEM (*n*)	A/J low fat, Mean ± SEM (*n*)	A/J high fat, Mean ± SEM (*n*)	Conclusion: B6: HF versus LF
Plasma glucose (mg/dl)	*72.2 ± 6.5 (5)*	*97.6 ± 3.7 (8)*	39.9 ± 5.8 (5)	45.8 ± 6.4 (5)	*Elevated glucose*
Insulin (ug/l)	*1.1 ± 0.4 (5)*	*4.2 ± 0.3 (5)*	0.8 ± 0.1 (5)	0.5 ± 0.03 (5)	*Hyperinsulinemia*
Triglyceride–plasma (mg/dl)	74.6 ± 7.9 (8)	68.1 ± 6.7 (9)	107.3 ± 14.4 (5)	46.8 ± 14.9 (5)	NS
Triglyceride–hepatic (mg/gram liver)	nd; 30[a]	165.50 ± 22.02 (5); 110[a]	nd; 58.4[b]	nd; 77.8[b]	*Steatosis*
ALT (U/l)	*19.30 ± 3.26 (5)*	*80.8 ± 1.9 (8)*	49.4 ± 14.7 (5)	28.3 ± 5.1 (5)	*Liver injury*
Hepatic TNFα (pg/mg protein)	*38.0 ± 2.0 (7)*	*99.83 ± 15.48 (8)*	39.8 ± 5.8 (5)	45.8 ± 6.5 (5)	*Liver injury*
CYP2E1/HSC70 (liver at 500 days)	0.90 ± 0.20 (8)	1.4 ± 0.40 (6)	1.5 ± 0.5 (5)	1.1 ± 0.2 (5)	NS
SREBP-1c mRNA/18SrRNA	1.34 ± 0.32 (4)	0.28 ± 0.06 (4)	1.0 ± 0.27 (4)	0.73 ± 0.28 (4)	NS
ACC-1 mRNA/18S rRNA	0.51 ± 0.08 (4)	0.07 ± 0.01 (4)	0.5 ± 0.14 (4)	0.17 ± 0.04 (4)	*Reduced lipogenesis*
FAS mRNA/18S rRNA	1.18 ± 0.49 (4)	0.15 ± 0.70 (4)	1.3 ± 0.56 (4)	0.27 ± 0.03 (4)	NS
AOX mRNA/18S rRNA	0.06 ± 0.01 (4)	0.02 ± 0.01 (4)	0.02 ± 0.01 (4)	0.03 ± 0.01 (4)	NS
CPT-1 mRNA/18S rRNA	0.06 ± .01 (4)	0.03 ± 0.01 (4)	0.7 ± 0.03 (4)	0.06 ± 0.01 (4)	NS
LCAD mRNA/18S rRNA	0.05 ± 0.01 (4)	0.03 ± 0.01 (4)	0.07 ± 0.02 (4)	0.06 ± 0.02 (4)	NS

Italic values denote statistically significant differences at $P < 0.05$ after Bonferroni correction for multiple testing. SEM, standard error of the mean and *n*, sample size. See text for definition of trait abbreviations.
[a]ref 12, [b]ref 53.

GSEA analysis suggested that mouse genes whose orthologs are located on human chromosome 4q25 were over-represented (fdr < 0.001) among up-regulated genes in diet-induced HCCs, with the combination of up-regulated genes varying among tumor samples (Fig. 7). In humans, chromosome 4q is frequently involved in chromosomal abnormalities in HCCs, the majority of which involve deletions rather than amplifications (18). However, chromosomal amplification of 4q is commonly associated with resistance to the chemotherapy drug cisplatin, to which HCCs are often resistant (19).

HCC mRNA profiles in humans and mice

We compared the expression profiles for diet-induced HCCs in our model with HCCs in humans and other mouse models using an updated list of orthologous genes (20). This updated list introduced 1292 new genes bringing the total number of genes to 5328. Hierarchical clustering was largely consistent with the original report (20) despite addition of many orthologous genes that have been newly annotated since the original report (Fig. 8A). Three major HCC clusters were found, only two of which contained human HCC samples. Diet-induced HCCs were found in both subclasses of human HCCs, suggesting that expression profiles for these HCCs in mice were highly similar to the two common HCC subclasses in humans, rather than representing profiles that are unique to diet-induced tumorigenesis in mice.

To identify pathways and networks that are involved in these two distinct subclasses of HCC, we first averaged the gene expression values for the 5328 orthologous genes (see above) for tumors 16, 20, 23 and 26, and then compared these average expression levels to the expression of the same gene in the corresponding liver sample. For the four mouse tumors that clustered with human HCC subclass B, the top-ranked network centered on Myc (*P*-score = 46; Fig. 8B), and the second and third ranked networks centered on NFκB (*P*-score = 44) and TGFβ (*P*-score = 44), respectively (not shown). Interestingly, HCCs in Myc transgenic mice also clustered with human HCC subclass B (20). In contrast, the top-ranked network for tumor 19, which clustered with HCC subclass A, centered on NFκB (*P*-score = 44; Fig. 8C), and the second and third ranked networks centered on IGF2/FGF2 (*P*-score = 44) and PPARα/PPARγ (*P*-score = 43), respectively (data not shown). Previous studies showed that engineered variants in genes such as Myc (20), TGFβ (21), IGF2 (22) and PPARα (23) increase susceptibility to HCCs.

Finally, we tested whether liver damage in NASH and HCCs resembles liver regeneration, a reversion to fetal developmental programs, or another kind of proliferation. In particular, we compared expression profiles for diet-induced NASH and HCCs with published profiles for liver regeneration and for liver development (24). Interestingly, diet-induced liver disease clustered separately from regenerating and developing liver, suggesting that NASH and HCCs represent a distinct class of hyper-proliferation (Fig. 9).

miRNA expression profiles

We next conducted three studies of miRNA expression in diet-induced HCCs and corresponding liver samples. First, expression profiles for all known miRNAs ($n = 572$) in miRBase v10.1 (25) revealed differential expression for only four miRNAs between pairs of tumor and liver. mmu-miR-31, mmu-miR-146 and mmu-miR-182 were up-regulated in the HCCs versus liver, and mmu-miR-191 was down-regulated. For each up-regulated miRNA, differential expression was validated with qRT–PCR (Supplementary Material, Fig. S1). We next sought to classify mouse tumors in subclasses A and B by clustering their miRNA expression patterns. As with the mRNA analysis, hierarchical clustering,

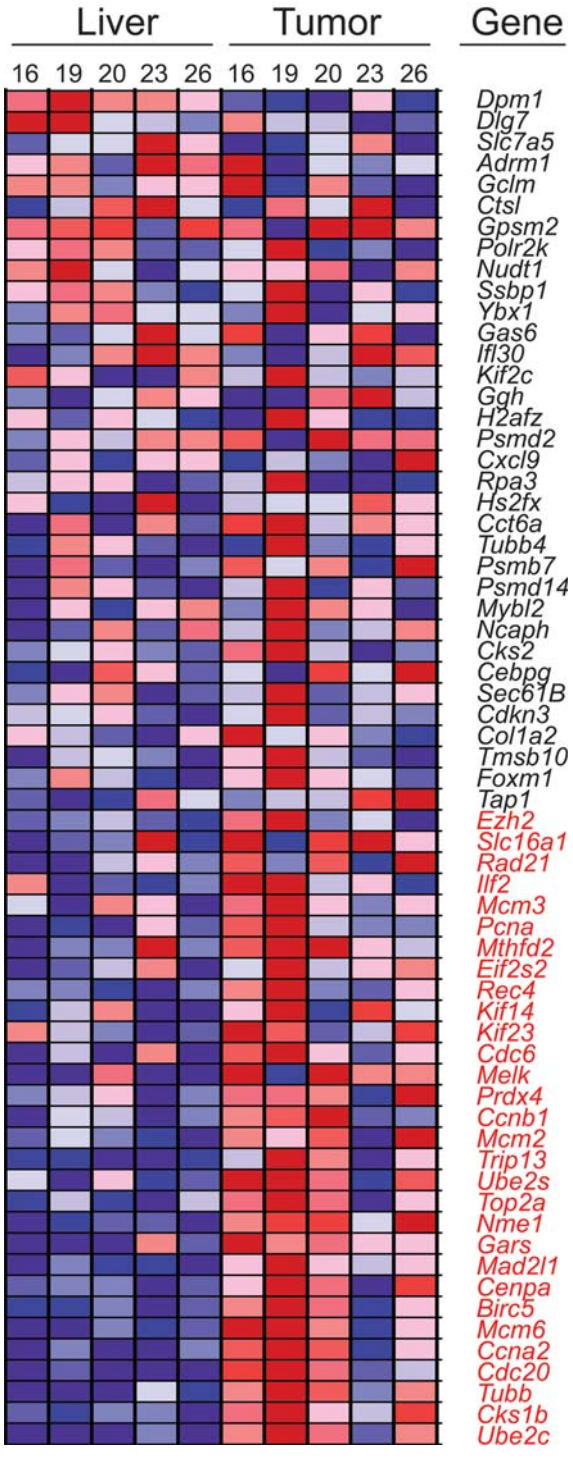

Figure 6. Gene expression pattern of HCCs resemble an undifferentiated cancer. Each column represents one sample (chip) and each row represents one gene. The range of colors (red to blue) corresponds to the range of expression values (high to low). Genes contributing to the core enrichment are shown in red.

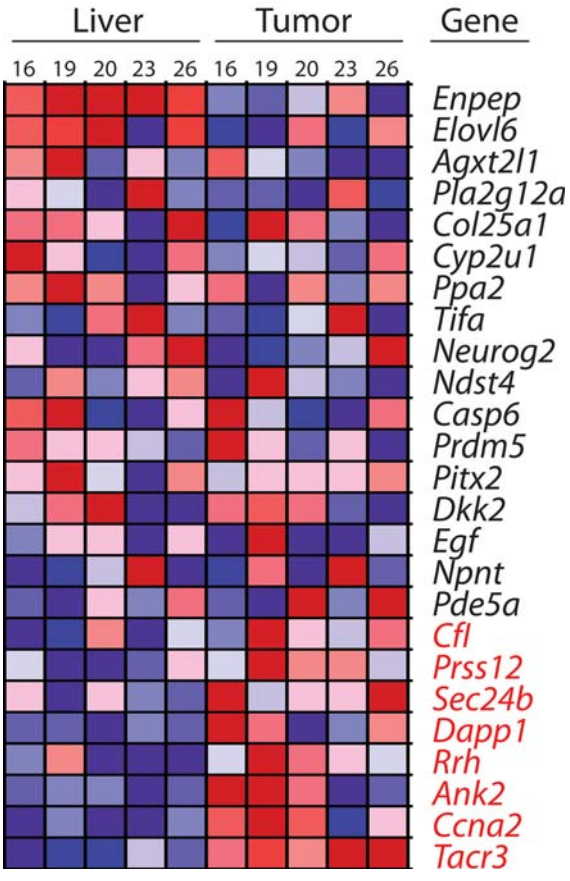

Figure 7. Genes on human 4q25 are over-represented among those that are up-regulated in HCCs. Each column represents one sample and each row represents one gene. The range of colors (red to blue) corresponds to the range of expression values (high to low). Genes contributing to the core enrichment are shown in red.

with Pearson's correlation and average linkage, showed that tumor 19 was the most distinct of the tumors 16, 19, 23 and 26 (not shown). Finally, the subclass B tumor (tumor 19) uniquely over-expressed 19 miRNAs relative to normal liver and to subclass A tumors (Fig. 10A). Of these 19 miRNAs, 16 are localized within a 62 Kb interval on chromosome X between 64.02 and 64.10 Mb (Ensembl release 50) (Fig. 10B). This 62 Kb interval was not amplified in genomic DNA isolated from tumor 19, suggesting that these miRNAs are transcriptionally co-regulated. The mRNA targets of these 19 recently discovered miRNAs have not yet been reported.

To identify candidate mRNA targets of the miRNAs, we examined the overlap of the mRNAs with the target genes predicted by miRANDA (http://microrna.sanger.ac.uk). Sets of predicted target genes were compiled with miRANDA using various significance cutoff values to decrease the false-positive rate with increasingly stringent filters (Supplementary Material, Table S2). The intersect of miRANDA predicted mRNA targets and inversely correlated mRNAs was compared with the intersect of miRANDA predicted targets and all mRNAs to determine whether the inversely correlated mRNAs were enriched for putative direct targets (Supplementary Material, Table S2). By increasing the stringency from 0.05 to 0.0005, the number of predicted mRNA targets decreased from 296 to 58 mRNAs and comparing the intersections showed a fold-enrichments from 1.7 to 2.4 (Supplementary Material, Table S2). At the most stringent level, the 58

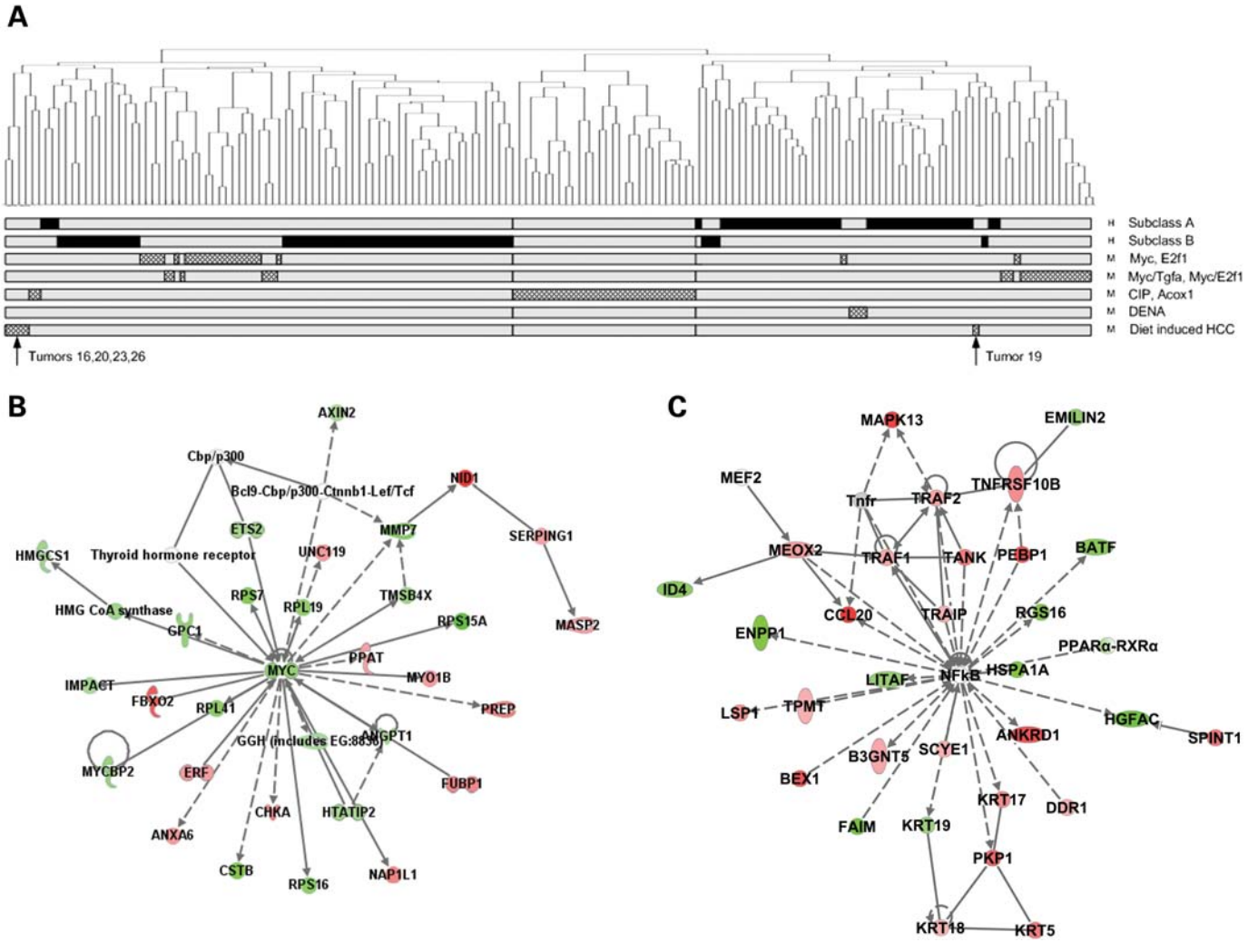

Figure 8. mRNA profiles. (**A**) Hierarchical clustering of mRNA expression profiles of human HCCs and mouse models. The analyses were augmented with newly identified orthologous genes that were identified since the original report (20); see Lee *et al*. (20) for details about the data and definition of gene symbols and carcinogen treatments. Colored cells (black for humans and gray for mice) were used to show the subclass membership. Subclass membership for diet-induced HCCs is shown at the bottom. H, human; M, mouse. (**B**) Myc network. The Myc network was the top-ranked network for the tumors (15,19,22,25). (**C**) NFκB network. NFκB is the top-ranked network for HCC19 but not the four others.

genes occurred preferentially ($P < 0.001$) in three networks—liver necrosis and cell death, cardiac degeneration and cardiac necrosis and cell death (Supplementary Material, Table S3).

DISCUSSION

Given the increasing incidence of HCCs and absence of effective therapies, the need is urgent to identify biomarkers of inherited risk and disease status as well as treatments that prevent or reverse adverse outcomes. HCCs in humans have remarkably diverse etiologies that presumably converge on a smaller number of down-stream pathogenic pathways. Animal models, which typically involve chemical carcinogenesis, drug exposure or genetic engineering, have been instrumental for dissecting the molecular pathways that contribute to carcinogenesis in the liver (20,21,26). These models test hypotheses about the involvement of specific genes, but do not capture the genetic and environmental complexity of HCC tumorigenesis. Several inbred strains of mice have been used to study gene-diet interactions in metabolic diseases. In particular, C57BL/6J but not A/J inbred mice are susceptible to diet-induced obesity, dyslipidemia and insulin resistance (6,7). In these models, multiple genes and gene-environment interactions that control disease susceptibility might more closely reflect the natural circumstances in NASH and HCC pathogenesis.

We found that long-term exposure to a high-fat diet in a genetically susceptible C57BL/6J inbred strain of laboratory mouse led to NASH and to high rate of spontaneous HCCs. This model shows classic histological, biochemical and molecular features of both common subclasses of HCCs in humans. Similarly, despite long-term exposure to a high-fat diet, the A/J strain provides a contrasting model of genetically determined resistance to NASH and HCCs. Together these two strains afford an unprecedented opportunity to study the ways

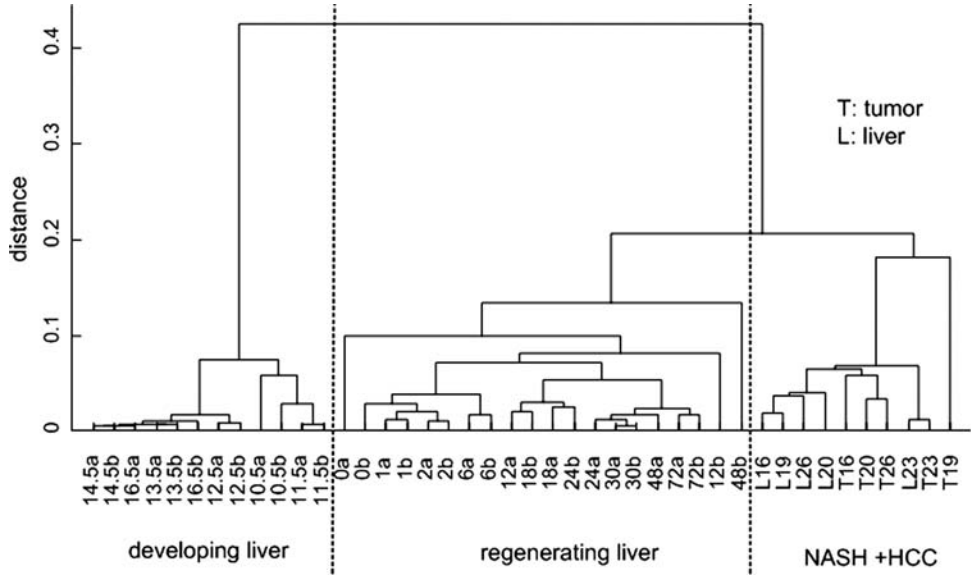

Figure 9. Hierarchical analysis of mRNA expression patterns in developing liver, regeneration liver and diet-induced HCCs.

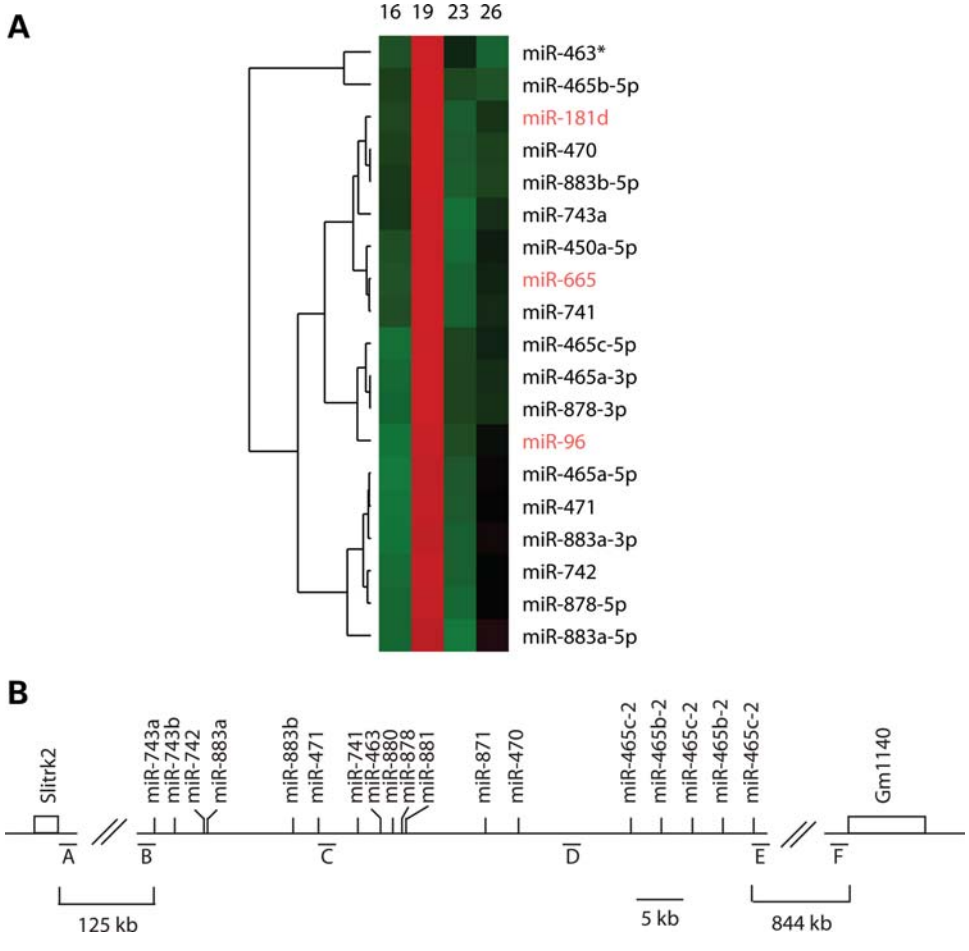

Figure 10. X-linked miRNA cluster. (**A**) Hierarchical cluster analysis of mRNA expression in the four HCC tumors. miRNAs (black) are located in the X-linked cluster and those in red are located elsewhere in the genome. (**B**) Sequence-based map of the X-linked miRNA cluster. (A)–(**E**) shows the location of PCR primers that were used to test for genomic amplification (Supplementary Material, Table S1). *Slitrk2* and *Gm1140* are the closest flanking genes on the proximal and distal sides, respectively. Scale bar represents 5 kb.

in which a high-fat diet leads to liver damage and malignant transformation of liver cells.

Diet-induced obesity has many comorbidities including pathologies of diverse organ systems as well as cancers of the liver, kidney, pancreas, colon and esophagus in both females and males, and other sites such as breast and uterus in females (27,28). In particular, non-alcoholic pancreatic disease has been described in leptin-deficient mice that were fed a 15% high-fat diet, but pancreatic cancer was not observed perhaps because the 8 week exposure period was too short (29). In the present study, visual and histological examination of the pancreas did not reveal evidence either for lipid accumulation or inflammation, or for pancreatic cancer in either C57BL/6J or A/J males at the end of our ~500 day study. In addition, no other organs showed gross evidence of pathologies. Thus, long-term exposure to saturated high-fat diet induced liver cancer, but not other cancers or other obvious pathologies in C57BL/6J or A/J males.

Although part of many models, the necessity of cirrhosis in HCC pathogenesis is questionable (3). In fact, cirrhosis is sometimes not found in HCCs (8–10). In addition, leptin-deficient mice show steatosis and HCCs but not inflammation or cirrhosis (30,31). In the livers with NASH and diet-induced HCCs described here, cirrhosis was never extensive and was in some cases not evident (Fig. 3). Thus, cirrhosis does not appear to be an essential step in some classes of HCC tumorigenesis.

HCC associated with NASH is thought to result from a series of steps that begin with lipid accumulation in the liver, either from dietary lipids or from lipolysis, then peroxidation of these lipids triggers inflammation (hepatitis) and ultimately this continuous process induces development of HCCs. Diets that are high in saturated fats as well as genetic variants in key genes in lipid metabolism exacerbate this process (8–10). For example, dietary fat increases pro-inflammatory responses, exacerbating liver injury (10,11). In addition, PPARα senses excess free fatty acids and up-regulates programs for fatty acid disposal and PPARα variants increase risk for HCCs in mouse models (23). HCCs can also result from genetic variants affecting cell signaling (Akt, E-cadherin, β-catenin, ERK, MEK, MET, PI3K, Ras, Rat, mTOR and Wnt), cell cycle regulation (p16, p53, INK4, cyclin's and cdk's) and invasiveness (IEMT and TGFβ) (20,21,32,33). In humans and mouse models, several classes of HCCs have been described, suggesting that these various etiologies and genetic variants activate alternative pathogenic pathways (32–34). These classes show epithelial versus mesenchymal characteristics and differ both in their propensity to metastasis and invasiveness as well as response to EGFR inhibitors (35,36). In the diet-induced HCCs described here, one class, which corresponds to human HCC subclass B, was characterized by differential expression of genes involved in the Myc, NFκB and TGFβ networks, whereas the other class involved in the NFκB, IGF2/FGF2 and PPARα/PPARγ networks (Fig. 8). An important challenge involves building a predictive model that integrates the ways in which these overlapping networks contribute to the alternative classes of HCCs. Another key question concerns whether these HCC subclasses represent different stages along a single pathogenic pathway, or related but alternative paths to tumorigenesis.

miRNAs are emerging as a new class of regulators of cancer development. We found several changes in the miRNA expression that are relevant to diet-induced HCCs. Three miRNAs showed up-regulation (miR-31, -146 and -182) and one showed down-regulation (miR-191) in HCCs versus corresponding livers with NASH. Interestingly, mmu-miR-31 is also up-regulated in colon cancers in humans (37) and differentially processed in liver cancer cell lines (38), whereas mmu-miR-146 is up-regulated in chronic lymphocytic leukemia (39) and papillary thyroid carcinoma (40). In addition, NFκB activates mmu-miR-146 expression which in turn negatively regulates the IRAK1 and TRAF6 in the TNFα signaling pathway of innate immunity (Fig. 8; see also refs. 20,41). In contrast, miR-191 is up-regulated in colon cancer in humans (42) and down-regulated in the diet-induced HCCs described here, but it is unclear whether these contrasting results reflect different functions of miR-191 in colon and liver cancers or differences in its regulation in humans and mice.

A cluster of miRNAs located on mouse chromosome X showed significant increases in expression levels, without amplification of the chromosome segment, in HCCs versus corresponding livers (Fig. 10). Although the mRNA targets of this recently reported X-linked miRNA cluster have not yet been identified, analysis of the intersection between computationally predicted mRNA targets for these X-linked miRNAs and mRNAs that showed reduced expression in tumor versus liver revealed a short-list mRNAs that are candidate mRNAs for these miRNAs (Supplementary Material, Tables S2 and S3). These genes are occurred preferentially in networks related to necrosis, apoptosis and degeneration (Supplementary Material, Table S3), all of which are relevant to NASH. Thus, a small number of miRNAs appear to be intimately involved in HCC tumorigenesis.

Considerable evidence shows that dietary factors affect occurrence and progression of various cancers (43,44). Few examples are known, however, where alternative diets reverse pathology and protect against cancer development. An important challenge is to find ways to reverse or stop progression of premalignant conditions to invasive tumors associated with diet-induced liver pathologies (45,46). We showed that simply switching to a diet that has low rather than high levels of saturated fats, even after onset of liver pathologies but before the development of dysplasia or carcinoma, reversed outcome, with switched mice being lean at the end of the study and with no evidence of NASH or HCCs. These studies suggest that diet modification might have important implications for HCC prevention in humans.

MATERIALS AND METHODS

Mice, husbandry and autopsy

A/J and C57BL/6J males were obtained from the Jackson Laboratory (Bar Harbor, Maine) or from our colonies at CWRU. Mice were weighed at 2 week intervals for 100 days starting at 35 ± 3 days of age and then once a month for the remainder of the study. They were also inspected regularly for signs of morbidity and disease. Mice were maintained at ~21°C in ventilated cages and on a 12 h light-dark cycle. At autopsy, mice were euthanized with isoflurane, weighed and the

nose-to-tail length measured; these were used to calculate BMI (g/cm^2). All procedures were approved by the CWRU Institutional Animal Care and Use Committee.

Diets

Mice were raised on one of two diets: high-fat diet (H; D12331: kcal—16% protein, 58% saturated fat, 26% carbohydrate, 0 ppm choline; Research Diets Inc., New Brunswick, NJ, USA; www.researchdiets.com) and low-fat diet [L; LabDiet 5010 autoclavable rodent chow: kcal—29% protein, 13% saturated fat (1.2% saturated fat), 59% carbohydrate, 2200 ppm choline; LabDiet, Richmond, IN, USA; www.labdiets.com]. We note that saturated fat was the most likely factor contributing to diet-induced metabolic disease and cancer; we also note that the substantial difference in the amount of choline was probably not a contributing factor because the H diet had significantly less than the L diet.

Histology

Formalin-fixed, paraffin-embedded tissues were sectioned (8 μ) and stained with hematoxylin and eosin (H&E). Masson's trichrome was used to visualize fibrosis.

Biochemical assays

Mice were anesthetized with isoflurane and blood samples were obtained from the retro-orbital sinus. Plasma was obtained with Microtainer plasma separator tubes (Becton Dickinson, Franklin Lakes, NJ, USA). Plasma and liver triglyceride levels were measured with the Triglyceride GPO reagent set (Pointe Scientific, Lincoln Park, MI, USA), glucose with a colorimetric assay using a Glucose Assay Kit (BioVision Research Products, Mountain View, CA, USA) and insulin with an Ultrasensitive Mouse Insulin ELISA enzyme immunoassay (Mercodia, Winston Salem, NC, USA). Serum samples were assayed for aspartate aminotransferase (AST) and alanine aminotransferase (ALT) with a commercially available enzymatic assay kit (Sigma-Aldrich, St Louis, MO, USA). Liver homogenates were assayed for TNFα peptide with an ELISA kit (Mouse Quantikine, R&D Systems, Minneapolis, MN, USA).

RNA extraction

Mice were euthanized with isoflurane. Tissues were collected and stored in RNAlater (Ambion). RNA was extracted using the Qiagen RNeasy mini-kit or the Qiagen miRNeasy mini-kit. RNA quality was assessed with a Bioanalyzer 2100 (Agilent) prior to microarray hybridization.

Real-time quantitative PCR

Single-strand cDNA was synthesized from 2 μg of total RNA with random hexamer primers and MMTV Reverse Transcriptase (Ambion, Austin, TX, USA). Real-time PCR was performed with a Chromo4 Cycler (MJ Research, Waltham, MA, USA), as previously described (47). The primers that were used for these studies are provided in Supplementary Material, Table S1. PCR was performed in the Chromo4 Cycler (MJ Research) with 40 cycles [15 min at 95°C; followed by 40 cycles of 30 s at 95°C, 30 s at 60°C, 45 s at 72°C and 30 s at 73°C (optimal read)]; followed by a 5 min extension at 72°C. 18S rRNA was used as a loading control. The relative amounts of the mRNAs were estimated with linear regression from the standard curves derivative maximum method with Opticon Monitor 3 software (MJ Research). Four mice were tested for each gene.

miRNA RT–PCR

miRNA expression was determined using TaqMan miRNA assays (Applied Biosystems, Foster City, CA, USA). The TaqMan miRNA Reverse Transcription Kit was used as indicated with 10 ng of total RNA as template. The ΔΔCt method was used to determine the miRNA expression levels relative to the control snoRNA 429. Each sample was done in quadruplicate.

Copy number variation

DNA was isolated using the Gentra Puregene tissue kit (Qiagen, Valencia, CA, USA) and DNA copy number was determined using the PerfeCta SYBR green super-mix (Quanta BioSciences, Gaithersburg, MD, USA). Primers were designed using Primer 3Plus to amplify a 70–200 bp fragment. Each primer pair (see Supplementary Material, Table S1) was tested for specificity by amplification and gel electrophoresis prior to qPCR. Genomic DNA (6.25 ng) was used in a 25 μl reaction with the following cycling conditions: 95°C for 3 min followed by 40 cycles of 10 s at 95°C and 45 s at 60°C followed by a melting curve analysis. Standard curves were generated using 2-fold dilutions of liver genomic DNA isolated from mouse B6–19 (range 1.6 ng–25 ng). Test samples were run in triplicate. Each PCR amplicon was normalized to Pomc to calculate the relative copy number.

mRNA microarray hybridization

Genome-wide mRNA expression levels were determined using the Affymetrix GeneChip Mouse Genome 430 2.0 array which contains 45 037 probes corresponding to over 39 000 transcripts. Hybridizations were carried out by the Gene Expression and Genotyping Facility of the Case Comprehensive Cancer Center.

miRNA microarray hybridization

Genome-wide miRNA expression profiling was performed by LC Sciences (Houston, TX, USA) as previously described (48). The miRNA microarray chip contained probes for 569 miRNAs, providing complete coverage of miRNAs present in miRBASE v10.1 (49). To minimize dye bias, two livers (15,22) and two tumors (18,25) were labeled with Cy3 and two livers (18,25) and two tumors (15,22) were labeled with Cy5.

Microarray data analysis

Signal values for the Affymetrix microarray data were background corrected and normalized with MAS5.0 (Affymetrix, Santa Clara, CA, USA). The expression value of each gene was represented by the average signal values of the corresponding probe sets. Expression analysis was performed with the VAMPIRE web-based microarray analysis suite using the 'paired model type' under default settings (14,15). The threshold for statistical significance was set to a Bonferroni corrected value of $P < 0.10$. To annotate genes with functions, the Goby annotation tool was used to query the Gene Ontology (GO) database (15,50). GSEA was performed using the MSigDB database v2.1 under default conditions except for the number of phenotype (tumor and liver) permutations ($n = 100$) (16).

Gene expression values of human HCC and other mouse models of HCC (accession numbers GSE1898 and GSE1897) were obtained from GEO (16). To compare with human tumor expression profiles, we extracted orthologous genes in humans and mice based on the current version of MGI Orthology (ftp://ftp.informatics.jax.org/pub/reports/index.html #orthology). Only orthologous genes present in all three platforms (NCI/ATC Hs-OperonV2, NCI/LMT Mm_FCRF_UniGEM2 and Affy GeneChip Mouse 430) were used. We averaged the signals from all liver samples as the control and used the ratio of individual tumors to the average liver sample for further data analysis. Before integrating this updated mouse data set with the human HCC data set, we standardized gene expressions to (0,1) distribution for each gene independently in each data set (13). Similarly, we extracted the nontrivial gene sets that had <30% missing expression data and at least 2-fold change between tumor and liver samples in at least 10% of samples across the panel of HCCs. This process yielded ~2500 orthologous genes. We then applied hierarchical clustering on this filtered data set with Matlab 2006a with average linkage and with the correlation coefficient as the distance measurement. Finally, ingenuity pathway analysis was used to identify pathways and networks that characterized different tumor types (cf. https://analysis.ingenuity.com/pa/info/help/Ingenuity_Network_Algorithm_Whitepaper_FINAL (2).pdf). Pathways were ranked according to the *P*-value for Fisher's exact test, which evaluates the number of differentially expressed genes in the data set versus all genes in the global dataset. *P*-scores for each network were calculated as $-\log_{10}$ (test *P*-value), i.e. a *P*-score of 45 corresponds to a Fisher's test *P*-value of 10^{-45}.

Signal values for the miRNA microarray data were analyzed with *t*-tests as described (48). The threshold for statistical significance was $P < 0.05$. Hierarchical clustering was also applied to the miRNA gene expression data using Cluster 3.0. Data were log transformed and normalized (0,1), and then average linkage hierarchical clustering was used. The output was visualized using Java Tree Viewer v1.1.1.

We applied *k*-means clustering ($k = 25$) to the normalized miRNA data set. One of the clusters involved 19 miRNAs, 16 of which are located on Chromosome X between 64.02 and 64.10 MB. To identify candidate mRNA targets of these 19 miRNAs, we combined the sequence-based target predictions of miRanda (51) with the *k*-means clustering algorithm ($k = 200$) that identified mRNAs whose expression levels were inversely correlated with miRNA expression levels. We hypothesized that mRNA levels that were inversely correlated with miRNA levels would be enriched for direct target genes of these miRNAs. Because clusters formed by *k*-means are mutually exclusive, each mRNA and miRNA can belong to only one cluster. As a result, the 19 miRNAs were divided into several clusters with nearly identical expression patterns. These clusters were merged to form a single cluster containing all 19 miRNAs and the inversely correlated mRNAs. This method is similar to a recent report (25).

Protein extraction, electrophoresis and western blotting

Proteins were isolated by homogenizing liver samples in 15 ml/g of ice-cold homogenizing buffer (20 mM Tris, pH 7.6, 0.1 mM EDTA, 0.5 mM EGTA, 1.0% Triton-X 100, 250 mM sucrose) with protease inhibitors (Mini Complete inhibitor mixture tablets from Roche Applied Science, Indianapolis, IN, USA) as described previously (52). Homogenates were centrifuged at 19 500*g* for 30 min at 4°C. The cytosolic fractions were used for western blotting. The concentration of protein was measured with the Bio-Rad Protein Assay using bovine serum albumin as a standard.

The samples were sonicated for 20 s and then 20 μg of protein was diluted with Laemmli sample buffer containing 100 mM Tris–HCl, pH 6.8, 20% β-mercaptoethanol, 4% SDS, 0.2% bromophenol blue and 20% glycerol, and then separated with 10% SDS–PAGE. Proteins were elecrophoretically transferred to Immobilon® polyvinylidene difluoride membranes and stained with Coomassie stain (45% methanol, 10% acetic acid, 2.5% Coomassie Blue R250) to ensure even loading. Non-specific protein binding to the filter was blocked with 5% milk, 10 mM Tris, 150 mM NaCl and 0.2% Tween 20. The filter was incubated with antibodies to CYP2E-1 (1.5 μg/ml) (Fitzgerald Industries International Inc., Concord, MA, USA) diluted in blocking buffer for 4 h at 22°C, followed by extensive washing with Tris-buffered saline (150 mM NaCl, 10 mM Tris and 0.05% Tween 20). The blots were incubated with secondary antibody linked to horseradish peroxidase (Santa Cruz Biotechnology, Santa Cruz, CA, USA) in 10 ml of blocking buffer for 1 h at 22°C and washed again. Immunoreactive proteins were detected using the Super-Signal Chemiluminescent Substrate® Kit and the density of the immunoreactive bands was measured with scanning densitometry. Normalization for loading differences was done with HSC70 1:16,000 (Santa Cruz Biotechnology) and secondary anti-mouse IgG-HRP conjugate antibody 1:10,000 (Santa Cruz Biotechnology).

SUPPLEMENTARY MATERIAL

Supplementary Material is available at *HMG* online.

ACKNOWLEDGEMENTS

We thank Dr Gretta Jacobs for help with the histology analysis and for discussing liver pathology with A.E.H.-B. and J.H.N., Dr Tim Kern for help with the histological analysis of the

pancreas and Drs Ken Tanabe and Jason Heaney for helpful discussions.

Conflict of Interest statement. None declared.

FUNDING

This work was supported in part by the National Institutes of Health (RR12305 to J.H.N., U54CA116867 to J.H.N. and N.A.B., DK075040 to C.M.C., AI068730 to J.D.L.) and the Charles B. Wang Foundation.

REFERENCES

1. Parkin, D.M. (2006) The global health burden of infection-associated cancers in the year 2002. *Int. J. Cancer*, **118**, 3030–3044.
2. Pang, R., Tse, E. and Poon, R.T. (2006) Molecular pathways in hepatocellular carcinoma. *Cancer Lett.*, **240**, 157–169.
3. Yang, S., Lin, H.Z., Hwang, J., Chacko, V.P. and Diehl, A.M. (2001) Hepatic hyperplasia in noncirrhotic fatty livers: is obesity-related hepatic steatosis a premalignant condition? *Cancer Res.*, **61**, 5016–5023.
4. Bugianesi, E. (2007) Non-alcoholic steatohepatitis and cancer. *Clin. Liver Dis.*, **11**, 191–207.
5. Thorgeirsson, S.S. and Grisham, J.W. (2002) Molecular pathogenesis of human hepatocellular carcinoma. *Nat. Genet.*, **31**, 339–346.
6. Surwit, R.S., Feinglos, M.N., Rodin, J., Sutherland, A., Petro, A.E., Opara, E.C., Kuhn, C.M. and Rebuffe-Scrivem, M. (1995) Differential effects of fat and sucrose on the development of obesity and diabetes in C57BL/6J and A/J mice. *Metabolism*, **44**, 645–651.
7. Singer, J.S., Hill, A.E., Burrage, L.C., Olszens, K.R., Song, J., Justice, M., O'Brien, W.E., Conti, D.V., Witte, J.S., Lander, E.S. *et al.* (2004) Genetic dissection of complex traits with chromosome substitution strains of mice. *Science*, **304**, 445–448.
8. Wanless, I.R. and Shiota, K. (2004) The pathogenesis of nonalcoholic steatohepatitis and other fatty liver diseases: a four-step model including the role of lipid release and hepatic venular obstruction in the progression to cirrhosis. *Semin. Liver Dis.*, **24**, 99–106.
9. Choi, S. and Diehl, A.M. (2005) Role of inflammation in nonalcoholic steatohepatitis. *Curr. Opin. Gastroenterol. Hepatol.*, **2**, 208–209.
10. Jou, J., Choi, S.S. and Diehl, A.M. (2008) Mechanisms of disease progression in nonalcoholic fatty liver disease. *Semin. Liver Dis.*, **28**, 370–379.
11. McClain, C.J., Mokshagundam, S.P., Barve, S.S., Song, Z., Hill, D.B., Chen, T. and Deaciuc, I. (2004) Mechanisms of non-alcoholic steatohepatitis. *Alcohol*, **34**, 67–79.
12. Biddinger, S., Almind, K., Miyazaki, M., Kokkotou, E., Ntambi, J.M. and Kahn, C.R. (2005) Effects of diet and genetic background on sterol regulatory element-binding protein-1c, stearoyl-CoA desaturase 1, and the development of the metabolic syndrome. *Diabetes*, **54**, 1314–1323.
13. Yin, M., Gabele, E., Wheeler, M.D., Connor, H., Bradford, B.U., Dikalova, A., Rusyn, I., Mason, R. and Thurman, R.G. (2001) Alcohol-induced free radicals in mice: direct toxicants or signaling molecules? *Hepatology*, **34**, 935–942.
14. Hsiao, A., Ideker, T., Olefsky, J.M. and Subramaniam, S. (2005) VAMPIRE microarray suite: a web-based platform for the interpretation of gene expression data. *Nucleic Acids Res.*, **33**, W627–W632.
15. Hsiao, A., Worrall, D.S., Olefsky, J.M. and Subramaniam, S. (2004) Variance-modeled posterior inference of microarray data: detecting gene-expression changes in 3T3-L1 adipocytes. *Bioinformatics*, **20**, 3108–3127.
16. Subramanian, A., Tamayo, P., Mootha, V.K., Mukherjee, S., Ebert, B.L., Gillette, M.A., Paulovich, A., Pomeroy, S.L., Golub, T.R., Lander, E.S. *et al.* (2005) Gene set enrichment analysis: a knowledge-based approach for interpreting genome-wide expression profiles. *Proc. Natl Acad. Sci. USA*, **102**, 15545–15550.
17. Rhodes, D.R., Yu, J., Shanker, K., Deshpande, N., Varambally, R., Ghosh, D., Barette, T., Pandey, A. and Chinnaiyan, A.M. (2004) Large-scale meta-analysis of cancer microarray data identifies common transcriptional profiles of neoplastic transformation and progression. *Proc. Natl Acad. Sci. USA*, **101**, 9309–9314.
18. Lau, S.H. and Guan, X.Y. (2005) Cytogenetic and molecular genetic alterations in hepatocellular carcinoma. *Acta Pharmacol. Sin.*, **26**, 659–665.
19. Carr, B.I. (2004) Hepatocellular carcinoma: current management and future trends. *Gastroenterology*, **127**, S218–S224.
20. Lee, J.S., Chu, I.S., Mikaelyan, A., Calvisi, D.F., Heo, J., Reddy, J.K. and Torgeirsson, S.S. (2004) Application of comparative functional genomics to identify best-fit mouse models to study human cancer. *Nat. Genet.*, **36**, 1306–1311.
21. Lee, J.S., Grisham, J.W. and Thorgeirsson, S.S. (2005) Comparative functional genomics for identifying models of human cancer. *Carcinogenesis*, **26**, 1013–1020.
22. Desbois-Mouthon, C., Cacheux, W., Blivet-Van Eggelpoel, M.J., Barbu, V., Fartoux, L., Poupon, R., Housset, C. and Rosmorduc, O. (2006) Impact of IGF-1R/EGFR cross-talks on hepatoma cell sensitivity to gefitinib. *Int. J. Cancer*, **119**, 2557–2566.
23. Tanaka, N., Moriya, K., Kiyosawa, K., Koike, K., Gonzalez, F.J. and Aoyama, T. (2008) PPARalpha activation is essential for HCV core protein-induced hepatic steatosis and hepatocellular carcinoma in mice. *J. Clin. Invest.*, **118**, 683–694.
24. Otu, H.H., Naxerova, K., Ho, K., Nesbitt, N., Libermann, T.A. and Karp, S.J. (2007) Restoration of liver mass after injury requires proliferative and not embryonic transcriptional patterns. *J. Biol. Chem.*, **282**, 11197–11204.
25. Creighton, C.J., Nagaraja, A.K., Hanash, S.M., Matzuk, M.M. and Gunaratne, P.H. (2008) A bioinformatics tool for linking gene expression profiling results with public databases of microRNA target predictions. *RNA*, **14**, 2290–2296.
26. Diehl, A.M. (2005) Lessons from animal models of NASH. *Hepatol. Res.*, **33**, 138–144.
27. Qian, Y. and Fan, J.G. (2005) Obesity, fatty liver and liver cancer. *Hepatobilliary Pancreat. Dis. Int.*, **4**, 173–177.
28. Hjartaker, A., Langseth, H. and Weiderpass, E. (2008) Obesity and diabetes epidemics: cancer repercussions. *Adv. Exp. Med. Biol.*, **630**, 72–93.
29. Mathur, A., Marine, M., Lu, D., Swartz-Basile, D.A., Saxena, R. and Zyromski, N.J. (2007) Nonalcoholic fatty pancreas disease. *HPB*, **9**, 312–318.
30. Li, Z., Soloski, M.J. and Diehl, A.M. (2005) Dietary factors alter hepatic innate immune systems in mice with nonalcoholic fatty liver disease. *Hepatology*, **42**, 880–885.
31. Swartz-Basile, D.A., Goldblatt, M.I., Ho Choi, S., Svatek, C., Tran, K., Nakeeb, A. and Pitt, H.A. (2006) Biliary lipids and cholesterol crystal formation in leptin-deficient obese mice. *HPB*, **8**, 386–392.
32. Tward, A.D., Jones, K.D., Yant, S., Cheung, S.T., Fan, S.T., Chen, X., Kay, M.A., Wang, R. and Bishop, J.M. (2007) Distinct pathways of genomic progression to benign and malignant tumors of the liver. *Proc. Natl Acad. Sci. USA*, **104**, 14771–14776.
33. Coulouarn, C., Gomez-Quiroz, L.E., Lee, J.S., Kaposi-Novak, P., Conner, E.A., Goldina, T.A., Onishchenko, G.E., Factor, V.M. and Thorgeirsson, S.S. (2006) Oncogene-specific gene expression signatures at preneoplastic stage in mice define distinct mechanisms of hepatocarcinogenesis. *Hepatology*, **44**, 1003–1011.
34. Kaposi-Novak, P., Lee, J.S., Gomez-Quiroz, L., Coulouarn, C., Factor, V.M. and Thorgeirsson, S.S. (2006) Met-regulated expression signature defines a subset of human hepatocellular carcinomas with poor prognosis and aggressive phenotype. *J. Clin. Invest.*, **116**, 1582–1595.
35. Sicklick, J.K., Choi, S.S., Bustamante, M., McCall, S.J., Perez, E.H., Huang, J., Li, Y.X., Rojkind, M. and Diehl, A.M. (2006) Evidence for epithelial-mesenchymal transitions in adult liver cells. *Am. J. Gastrointest. Liver Physiol.*, **291**, G575–G583.
36. Fuchs, B.C., Fujii, T., Dorfman, J.D., Goodwin, J.M., Zhu, A.X., Lanuti, M. and Tanabe, K.K. (2008) Epithelial-to-mesenchymal transition and integrin-linked kinase mediate sensitivity to epidermal growth factor receptor inhibition in human hepatoma cells. *Cancer Res.*, **68**, 2391–2399.
37. Slaby, O., Svoboda, M., Fabian, P., Smerdova, T., Knoflickova, D., Bednarikova, M., Nenutil, R. and Vyzula, R. (2007) Altered expression of miR-21, miR-31, miR-143 and miR-145 is related to clinicopathologic features of colorectal cancer. *Oncology*, **72**, 397–402.

38. Lee, E.J., Baek, M., Gusev, Y., Brackett, D.J., Nuovo, G.J. and Schmittgen, T.D. (2008) Systematic evaluation of microRNA processing patterns in tissues, cell lines, and tumors. *RNA*, **14**, 35–42.
39. Calin, G.A., Ferracin, M., Cimmino, A., Di Leva, G., Shimizu, M., Wijcik, S.E., Iorio, M.V., Visone, R., Sever, N.I., Fabbri, M. *et al.* (2005) A microRNA signature associated with prognosis and progression in chronic lymphocytic leukemia. *N. Engl. J. Med.*, **353**, 1793–1801.
40. He, H., Jazdzewski, K., Li, W., Livanarachchi, S., Nagy, R., Volinia, S., Calin, G.A., Liu, C.G., Franssila, K., Suster, S. *et al.* (2005) The role of microRNA genes in papillary thyroid carcinoma. *Proc. Natl Acad. Sci. USA*, **102**, 19075–19080.
41. Taganov, K.D., Boldin, M.P., Chang, K.J. and Baltimore, D. (2006) NF-kappaB-dependent induction of microRNA miR-146, an inhibitor targeted to signaling proteins of innate immune responses. *Proc. Natl Acad. Sci. USA*, **103**, 12481–12486.
42. Xi, Y., Formentini, A., Chien, M., Weir, D.B., Russo, J.J., Ju, J., Kornmann, M. and Ju, J. (2006) Prognostic values of microRNAs in colorectal cancer. *Biomark Insights*, **2**, 113–121.
43. Iso, H. and Kubota, Y.Japan Collaborative Cohort Study for Evaluation of Cancer. (2007) Nutrition and disease in the Japan Collaborative Cohort Study for Evaluation of Cancer (JACC). *Asian Pac. J. Cancer Prev.*, **8**, S35–S80.
44. Demark-Wahnefried, W., Rock, C.L., Patrick, K. and Byers, T. (2008) Lifestyle interventions to reduce cancer risk and improve outcomes. *Am. Fam. Physician*, **77**, 1573–1578.
45. Felsher, D.W. (2004) Reversibility of oncogene-induced cancer. *Curr. Opin. Genet. Dev.*, **14**, 37–42.
46. Hino, O. (2005) Intentional delay of human hepatocarcinogenesis due to suppression of chronic hepatitis. *Intervirology*, **48**, 6–9.
47. Millward, C.A., Heaney, J.D., Sinasac, D.S., Chu, E.C., Bederman, I.R., Gilge, D.A., Previs, S.F. and Croniger, C.M. (2007) Mice with a deletion in the gene for CCAAT/enhancer-binding protein beta are protected against diet-induced obesity. *Diabetes*, **56**, 161–167.
48. Tay, Y.M., Tam, W.L., Ang, Y.S., Guaghwin, P.M., Yang, H., Wang, W., Liu, R., George, J., Ng, H.H., Perera, R.J. *et al.* (2008) MicroRNA-134 modulates the differentiation of mouse embryonic stem cells, where it causes post-transcriptional attenuation of Nanog and LRH1. *Stem Cells*, **26**, 17–29.
49. Griffiths-Jones, S., Grocock, R.J., van Dongen, S., Bateman, A. and Enright, R.J. (2006) miRBase: microRNA sequences, targets and gene nomenclature. *Nucleic Acids Res.*, **34**, D140–D144.
50. Ashburner, M., Ball, C.A., Blake, J.A., Botstein, D., Butler, H., Cherry, J.M., Davis, A.P., Dolinski, K., Dwight, S.S., Eppig, J.T. *et al.* (2000) Gene Ontology: tool for the unification of biology. *Nat. Genet.*, **25**, 25–29.
51. John, B., Enright, A.J., Aravin, A., Tuschi, T., Sander, C. and Marks, D.G. (2004) Human microRNA targets. *PLoS Biol.*, **2**, e363.
52. Croniger, C.M., Millward, C., Yang, J., Kawai, Y., Arinze, I.J., Liu, S., Harada-Shiba, M., Chakravarty, K., Friedman, J.E., Poli, V. *et al.* (2001) Mice with a deletion in the gene for CCAAT/enhancer-binding protein beta have an attenuated response to cAMP and impaired carbohydrate metabolism. *J. Biol. Chem.*, **276**, 629–638.
53. Millward, C., Burrage, L., Sinasac, D.S., Kawasoe, J.H., Hill-Baskin, A.E., Gornicka, A., Hsieh, C.W., Pisano, S., Nadeau, J.H. and Croniger, C.M. (2009) Genetic factors for resistance to diet-induced obesity and associated metabolic traits on mouse chromosome 17. *Mammal. Genome*, **20**, 71–82.